NUMERICAL MODELING OF A CAPACITIVE PROBE FOR MEASURING THE WATER LAYER THICKNESS IN HORIZONTAL AIR-WATER TWO-PHASE FLOWS

Emerson dos Reis, emersonr@ifsp.edu.br
Federal Institute of Education, Science and Technology of São Paulo, IFSP, Campus of São João da Boa Vista – Zip. Code 13872-551, São João da Boa Vista, S. P., Brazil.

Abstract. *Gas-liquid flows in pipelines is a complex issue. They determine several important characteristics of the transportation process. Nowadays, when the gas and liquid components are dielectric such as gas-mineral oil, air-deionized water or a gas-liquid mixture of some hydrocarbon refrigerant, the capacitive probing is a very prominent technique to study and control those two-phase flows. Typically, a capacitive probe is non-intrusive and has, basically, a source-sensing pair and guard electrodes placed on the outer surface of a dielectric pipe section and connected to a capacitance transducer circuit, with a metallic shield screen to avoid external interference. The geometrical configuration of electrodes determines the performance of the whole measurement system and, therefore, and it is the key when applying this technique in multiphase flows. Therefore, the electrodes' design must be focused in the flow regimes to be monitored and in the quantity of interest that can be volumetric such as the holdup of gas or liquid, or linear such as the liquid layer thickness formed into the flow. In this work, the probe proposed by dos Reis and Goldstein (2005) for measuring the water layer thickness in horizontal air-water flow was studied theoretically by FEM - Finite Element Method in search of understand the electrical phenomenon around the electrodes. In addition, its performance was evaluated theoretically in the presence of a conductive liquid phase, which is a subject of interest of many researchers around the world. Results were sufficient to study the probe's response with different design parameters, extending the information about this probe.*

Keywords*: Gas-liquid, Two-phase, Flow, Capacitance, Probe*

1. INTRODUCTION

The occurrence of gas-liquid flows in pipelines is very frequent in energy, chemical, food, and petroleum industries. Being the most impressive characteristic of them the number of different flow patterns or regimes that may be present. Flow regimes are represented by the spatial arrangement of each phase into the pipe, which depends on the volumetric flow, physical properties of phases, geometry of the pipe and gravity (Taitel and Barnea, 1976). They determine the overall performance of the equipment or transportation process, and dedicated instrumentation has expressive importance on their study, evaluation and control.

In a horizontal pipeline and with low or moderate flow velocities, the gravity acts trying to separate the gas from the liquid. The gas accumulates in the upper section and the liquid in the lower section of the pipe, generating a liquid layer. Such flow regimes are called stratified smooth, wavy and slug flow (Taitel and Barnea, 1976).

In literature, several authors presented different non-intrusive techniques for measuring the water layer thickness in gas-liquid flows, which should be optical, ultrasonic or capacitive (Keska and Fernando, 1992). The capacitive technique has some advantages since it is of low cost and robust, and the dielectric permittivity of gas is many times different from the liquid mainly when it is the water.

This technique is based on the measurement of the capacitance due to the electric field formed between a source-sensing pair of electrodes, which is dependent of the effective dielectric permittivity of the medium around them including the multiphase flow, being possible different configurations of electrodes for capacitive probes (Kendoush and Sarkis, 1995, Yang, 1996).

The electrodes' configuration determines the performance of the whole measurement system and, therefore, it is the key for use this technique in multiphase flows. The electrodes' design must be focused in the flow regimes to be monitored and in the quantity of interest that can be volumetric such as the holdup of gas or liquid, or linear such as the liquid layer thickness.

dos Reis and Goldstein (2005) proposed a capacitive probe for measuring the water layer thickness of air-water horizontal flows. The authors reported experimental data from the probe's static calibration and testing under several different flow conditions. However, little attention was paid to the study of the electric phenomenon into the probe. More recently, the authors published a study about dynamic characteristics of such two-phase flows by using this probe (dos Reis and Goldstein, 2010). They discussed details of their fluid dynamic from signal analysis in time and frequency domains and proposed a technique for flow regime identification that can be used in on-line applications.

Hence, this work has the following two goals: (1) to present a theoretical study about a capacitance probe proposed by dos Reis and Goldstein (2005) by using the FEM – Finite Element Method -, extending the information about this probe; and (2) to evaluate theoretically the response of this probe on the presence of a conductive liquid, which is also a subject of interest of several researcher around the world (Demori *et al*., 2010, Heidari *et al*., 2011).

2. PROBE´S DESCRIPTION

Figure 1 shows a sketch of the probe's section. It has a pair of source-sensing electrodes with the same θ. Both are assembled on the outer surface of the pipe of radius R_e equally separated by $e = R_e\ (\pi - \theta)$. The mounting angle β determines the position of the source-sensing pair of electrodes around the pipe perimeter in relation to the gravity g. There is a liquid layer of thickness h_L in the bottom region into the pipe. A shield screen of radius R_b involves the whole measurement section to avoid external interferences.

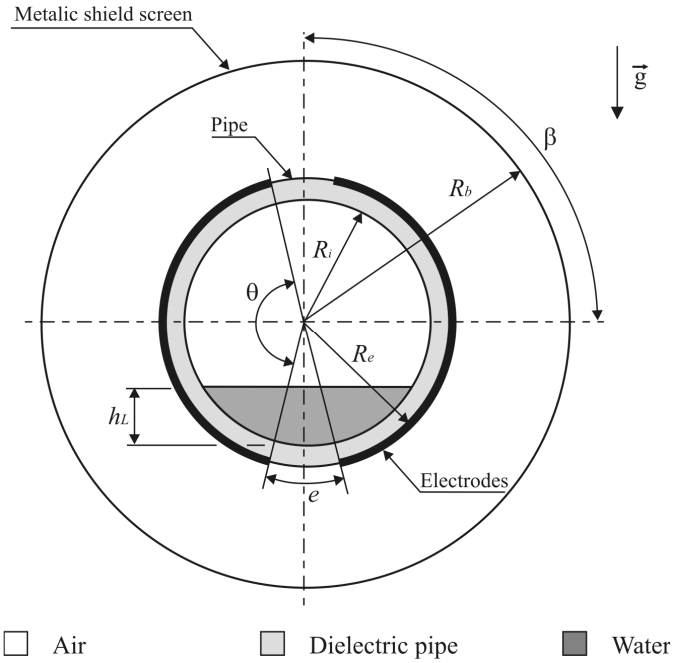

Figure 1. Sketch of the probe's section

In an AC based circuit, a sinusoidal signal is applied to the source electrode while the sensing electrode is connected to input of a capacitance transducer circuit (Yang, 1996, dos Reis and Goldstein, 2005). In this work, the capacitive reactance between the source-sensing pair due to the capacitance C_x is related to the liquid layer thickness h_L.

For capacitive probes with external electrodes, the pipe must be of any dielectric material such as polymer, ceramic, glass, allowing the electric field cross the pipe's wall to the internal region where the flow occurs. In this work, a Plexiglas pipe was adopted.

3. MODELLING

Two-dimensional (2D) modeling of different configurations of capacitive probes was already discussed in details by several authors (Xie *et al.*, 1990, Tollefsen and Hammer, 1998). It is usually carried out under the following assumptions: (i) the fringing field effect due to the finite length of the electrodes are negligible, assuming that the electric field distribution remains the same for any plane perpendicular to the axial flow direction; (ii) flow component distribution does not change spatially along the pipe axial direction (at least not within the electrodes length); (iii) permittivity of the flow components remain constant and don't depend on the field, which assumes the linearity of permittivity for a given field. Assumptions (i) and (ii) are of particular interest for wavy and slug flow regimes since they present an air-water interface typically as a 3D surface.

Under these assumptions, the electric field in the electrode system shown in Fig. 1 is governed by the following Poisson's equation in the domain Ω delimited by the shield screen as a static field problem (Xie *et al.*, 1990):

$$\vec{\nabla}.\left[\varepsilon_o\ \varepsilon(\vec{r})\,\vec{\nabla}\Phi(\vec{r})\right] = 0 \quad in \quad \Omega \tag{1}$$

This equation was solved numerically by FEM in terms of the electrostatic potential $\Phi(\vec{r})$ for a given space-varying dielectric permittivity of the flow component distribution $\varepsilon(\vec{r})$ relative to $\varepsilon_o = 8.8542 \times 10^{-12}$ F/m the free-space

dielectric permittivity. Furthermore, the associated boundary conditions imposed by this measurement technique are the following:

$$\Phi(\vec{r}) = \begin{cases} V_s & \forall\, \vec{r} \subseteq \Gamma_1 \\ 0 & \forall\, \vec{r} \subseteq \Gamma_2 \\ 0 & \forall\, \vec{r} \subseteq \Gamma_b \end{cases} \tag{2}$$

Γ_1 and Γ_2 represent the spatial locations of source (1) and sensing (2) electrodes, and Γ_b represents the spatial locations of the external shield screen. V_s is the static electric potential applied to source electrode, while the shield screen is grounded. The same potential is applied to the sensing electrode due to the virtual ground condition imposed by the input circuit architecture of the capacitance transducer (Yang, 1996).

Relative dielectric permittivity of all four different materials were in the distribution of air (ε_{air} = 1.0), of Plexiglas (ε_{pipe} = 3.3), and of water (ε_{water} = 80.0), which were already used by other authors (Geraest and Borst, 1988). However, one must consider differences due to temperature and compositions of materials in practical situations.

After solving all node potentials, the capacitance C_x can be calculated numerically by Eq. (3), where Q is the electric charge sensed by the sensing electrode and $d\vec{\Gamma}$ is the infinitesimal length vector on Γ_2:

$$C_x = \frac{Q(\Gamma_2)}{V_s} = \frac{\varepsilon_o}{V_s} \oint_{\vec{r} \subseteq \Gamma_2} \varepsilon(\vec{r}) \vec{\nabla} \Phi(\vec{r}) \,.\, d\vec{\Gamma} \tag{3}$$

Five different computational programs were used to solve Eq. (1) by FEM and Eq. (3). The first one generated the input file to the mesh generation program from specified geometrical parameters, Fig. 1. The 'Easymesh' program from Niceno (2011) was used to generate meshes of triangular elements of three nodes with refinement around both electrodes' edges where the electric potential gradients were more intense, generating about 10,000 elements and 6,000 nodes as shown in Fig. 2 for θ = 2.97, β = π/2 radians and h_1/D_i = 0.5. The quality of the generated mesh was tested since more refinement produces the same numerical results (dos Reis, 2003).

The third program got the output files of 'Easymesh' and, by applying all boundary conditions, generated the input file to the FEM solver program that also calculated C_x. All computational programs were disposed by dos Reis (2003).

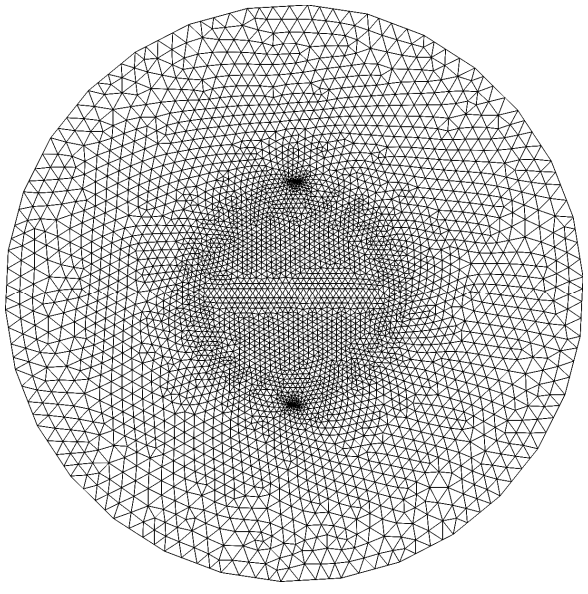

Figure 2. FEM mesh of triangular element with h_1/D_i = 0.5 and e = 3.55 mm

4. STRATEGY OF SIMULATION

In this work, a particular case of study had fixed pipe dimensions: R_e = 20.55 mm and R_i = 17.00 mm, which is an approximation of a 1 ½ inch commercial Plexiglas pipe. Hence, the pipe wall was 3.55 mm thick.

The mounting angle β was π/2 and 0 radians, placing the concave electrodes horizontally and vertically in relation to the gravity as show in Fig. 3. When β = 0, the source-sensing pair of electrodes was also permuted from the top to the bottom position to evaluate the effect of the sensing field that is higher near the sensing electrode (Xie *et al*., 1990).

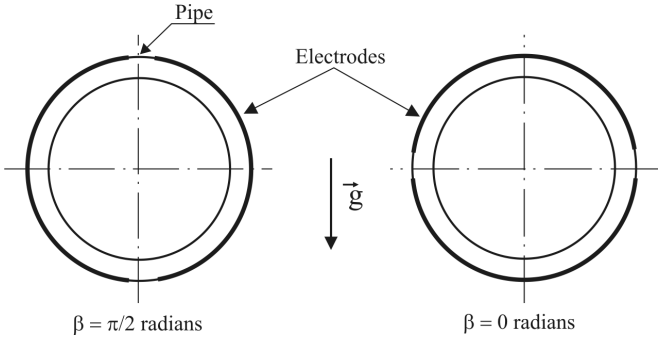

Figure 3. Mounting positions of the electrodes in relation to gravity

The angle θ had two different values: $\theta = 2.97$ radians or 170° ($e = 3.55$ mm) and $\theta = 2.09$ radians or 120° ($e = 21.52$ mm) to evaluate its effect on the performance of the probe.

For each combination of β and θ, simulations were performed with different values of the water layer thickness $h_L/D_i = 0$, 0.25, 0.5, 0.75 and 1.0, where $D_i = 2R_i$ is the internal diameter of the pipe, where $h_L/D_i = 0$ and 1.0 represent the pipe full filled of air and of water, respectively. Therefore, 20 different simulations were performed.

5. RESULTS AND DISCUSSION

Figure 4 shows distributions of the electrostatic potential $\Phi(\vec{r})$ in four cases with different combinations of θ and β, and the same $h_L/D_I = 0.5$. Equipotential lines are shown in black with colors from the strong red at highest to white at lowest potential. The electric field $\vec{E}$ lines (not showed) are perpendicular to the equipotential ones since $\vec{E} = -\nabla\Phi$.

Distributions of Φ between the source-sensing pair of electrodes and between the source electrode and the shield screen can be observed, being the source electrode at highest potential, $V_s = 4$ V (strong red), and sensing electrode and shield screen at lowest one of 0V (white) according to the boundary conditions of Eq. (2).

C_x is proportional to the amount of electric charge Q detected by the sensing electrode according to the Eq. (3), and Q is proportional to $\vec{\nabla}\Phi$ or $\vec{E}$. Therefore, as closer the equipotential lines as stronger $\vec{E}$ and, consequently, as higher the electric charge detected by the sensing electrode in that region, mainly in both regions near the electrodes' edges. In addition, the presence of water caused strong concentration of equipotential lines into the pipe's wall, as seen in (a) and (b) with $\beta = \pi/2$ radians. Differently, this effect isn't observed in (c) and (d) with stronger potential gradients (less than in (a) and (b)) had occurred into de air, with the bulk of water in almost the same potential of the adjacent electrode due to its high dielectric permittivity, with small differences caused by the presence of the pipe's wall. Therefore, C_x was higher in (a) and (b) than in (c) and (d) due to the wall influence on distributions of Φ, as shown in Figs. 6 and 8.

Around the electrodes' edges and into the annular region between the external pipe wall and the shield screen, the potential distribution was affected by all three metallic surfaces. Therefore, changes in the position of the shield screen in relation to the pipe, or of R_b, will also change the probe's response.

By reducing θ as shown from Fig. 4 (a) to (b) $\beta = \pi/2$ radians, $\vec{\nabla}\Phi$ or $\vec{E}$ became less intense around the electrodes' edges reducing C_x as seen in Fig. 6. This is better discussed next.

Although C_x is proportional to Q, it is also inversely proportional to the V_s according to Eq. (3), which means that the potential applied in the source electrode doesn't cause difference in C_x since variations of V_s generate proportionally more or less Q to be detected. Consequently, the capacitance depends only on the electrical properties of materials and geometric arrangement of the probe.

Cases of Fig. 4 can be represented by the equivalent electrical circuit shown in Fig. 5. It generates the total capacitance C_x to be measured, where (a) is the whole circuit with the flow section represented by a dashed rectangle, (b) represents the flow section circuit with $\beta = \pi/2$ radians and (c) the flow section with $\beta = 0$ radians.

In literature, the equivalent capacitance due to the flow C_{eq} is always related to the volumetric concentration (Jaworek *et al*., 2004). It depends on the effective permittivity, ε_e, of the medium between the electrodes. When plate voids are placed perpendicularly to the electrodes, it can be reduced to two virtual capacitances connected in parallel, one of permittivity of water and the other of gaseous phase as in Fig. 4 (a) and (b), then $\varepsilon_e = \alpha.\varepsilon_{air} + (1-\alpha).\varepsilon_{water}$, called parallel model, where α is the volumetric concentration of air. When plate voids placed are parallel to the electrodes, it can be reduced to two virtual capacitances connected in series as in Fig. 4 (c) and (d), then $1/\varepsilon_e = \alpha/\varepsilon_{air} + (1-\alpha)/\varepsilon_{water}$, called series model. The equivalent capacitance of the mixture between the electrodes can be presented as a certain function of the relative permittivity ε_e of the medium: $C_{eq} = C_{eq0}.f(\varepsilon_e)$ where C_{e0} is the equivalent capacitance for $\alpha = 1$, i.e., for the pipe without water inside. Jaworek *et al*. (2004) stated that for the parallel model, $C_{eq} = C_{eq0}.(\alpha + \varepsilon_{water}.(1-\alpha))$ for $\varepsilon_{air} = 1.0$. For series model, $C_{eq} = C_{eq0}/(\alpha + (1-\alpha)/\varepsilon_{water})$ as deduced. Therefore, C_{eq} is a linear function of α in

parallel model and non-linear function in the series model. However, in this work, we intent to measure the liquid layer thickness, h_L/D_1, and α isn't a linear function of this quantity as in Eq.(4), with small deviations from the linearity in both extremities with h_L/D_1 near to 0 and near to 1.0. Therefore, this fact justified the use of numerical simulation.

$$\alpha = \frac{1}{\pi}\left\{\pi - a\cos\left[1-2\frac{h_L}{D_1}\right] + \left(1-2\frac{h_L}{D_1}\right)\sqrt{1-\left(1-2\frac{h_L}{D_1}\right)^2}\right\} \tag{4}$$

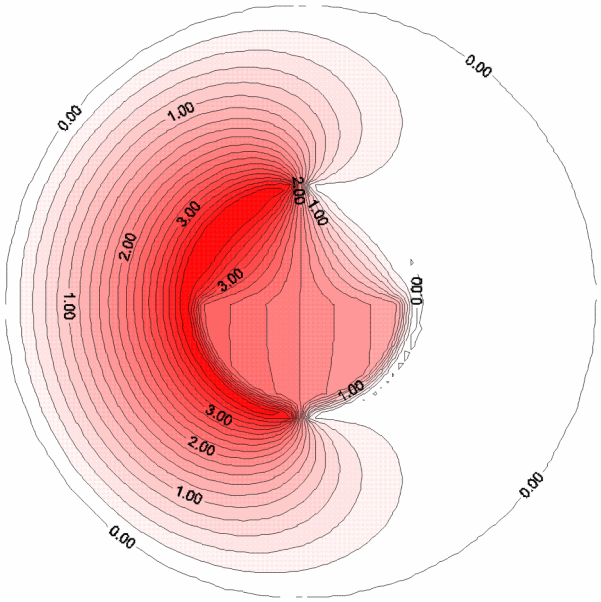

(a) β = π/2, θ = 2.97 rad and h_L/D_1 = 0.5

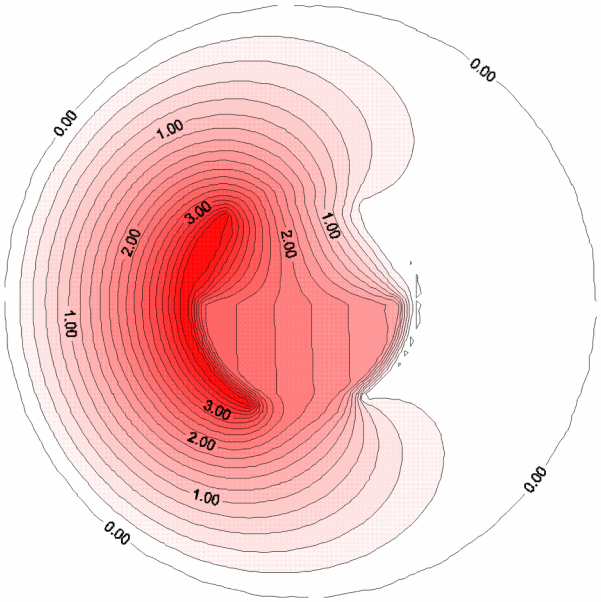

(b) β = π/2, θ = 2.09 rad and h_L/D_1 = 0.5

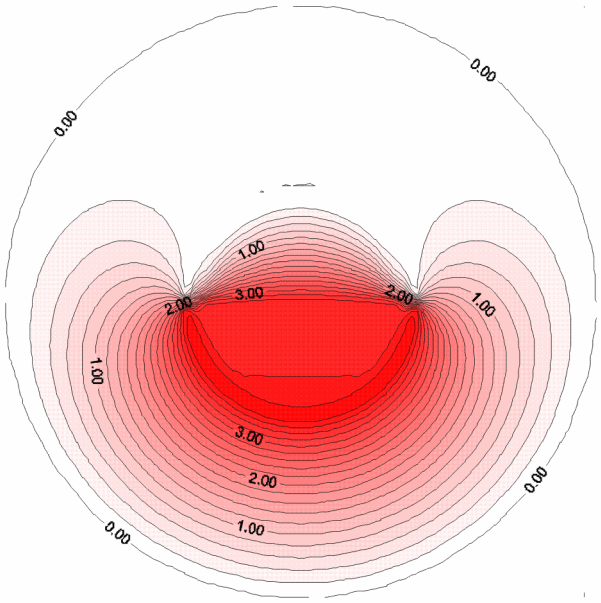

(c) β = 0, θ = 2.97 rad and h_L/D_1 = 0.5 - sensor electrode on the top

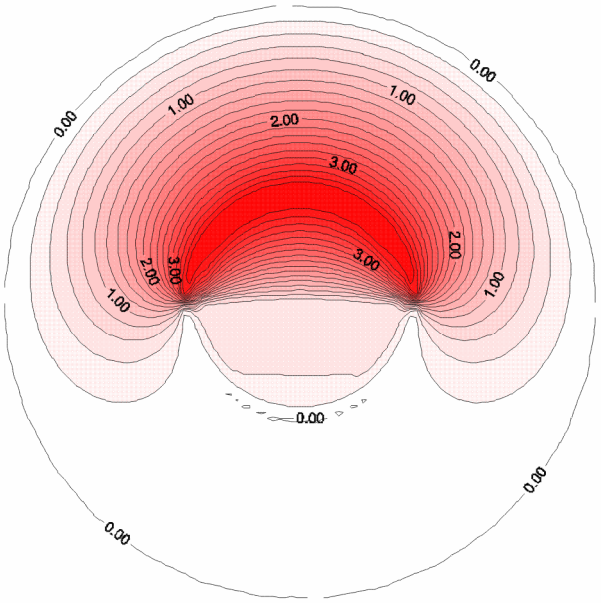

(d) β = 0, θ = 2.97 rad and h_L/D_1 = 0.5 - sensor electrode on the bottom

Figure 4. Distributions of the electric potential Φ for different combinations of θ and β and the same h_L/D_1 = 0.5

In Fig. 5 (b) and (c), $C_{air} = \alpha C_{eq0}$ in parallel model $C_{air} = C_{eq0}/\alpha$ in series model or and $C_{water} = (1-\alpha).\varepsilon_{water}.C_{eq0}$ in parallel model or $C_{water} = \varepsilon_{water}.C_{eq0}/(1-\alpha)$ in series model, they are the capacitances due to the air and water phases, respectively. One can observe the equivalent capacitance, C_{eq}, in the flow section depending on the position of the flow in relation to the gravity. $C_{eq} = C_{air} + C_{water}$ in (b) and $1/C_{eq} = 1/C_{air} + 1/C_{water}$ in (c), where. Capacitances due to pipe's

wall C_{wall} are important when $\beta = \pi/2$ rad, however, they can be disregarded when $\beta = 0$ rad since the same electric potential is present in both sides of C_{wall}. One can also observe that due to the high dielectric permittivity of the water, C_{water} is almost zero when $\beta = 0$. C_{scr} is the capacitance between the source electrode and the shield screen in the annular section, which should be independent of the liquid layer thickness, h_L/D_1, when $\theta = 2.97$ and dependent of it when $\theta = 2.09$ rad since Φ distributions are affected in the annular region due to the huge space between the electrodes, while the variant Φ due to the flow is kept into the flow section for largest electrodes. In Fig. 5 (a), the total capacitance $C_x = C_{scr}+C_{wall}.C_{eq}/(C_{wall} + C_{eq})$.

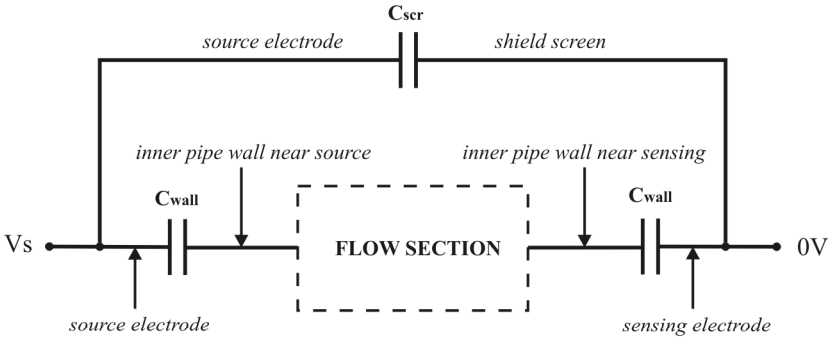

(a) Equivalent circuit

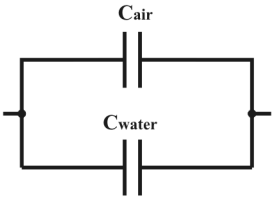

(b) Flow section: β = π/2 rad

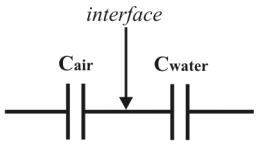

(b) Flow section: β = 0 rad

Figure 5. Electric equivalent circuit of the probe

Figure 6 shows C_x in picofarads per meter of electrode versus h_L/D_1 for $\beta = \pi/2$ radians, which is related to the Fig. 4 (a) and (b) represented by the central point in the graph with $h_L/D_1 = 0.5$. A linear response is always desired for instruments and, in this sense, some linearity on the central region of the graph with $\theta = 2.97$ radians can be observed (filled square), and also deviations from this linearity in both extremities.

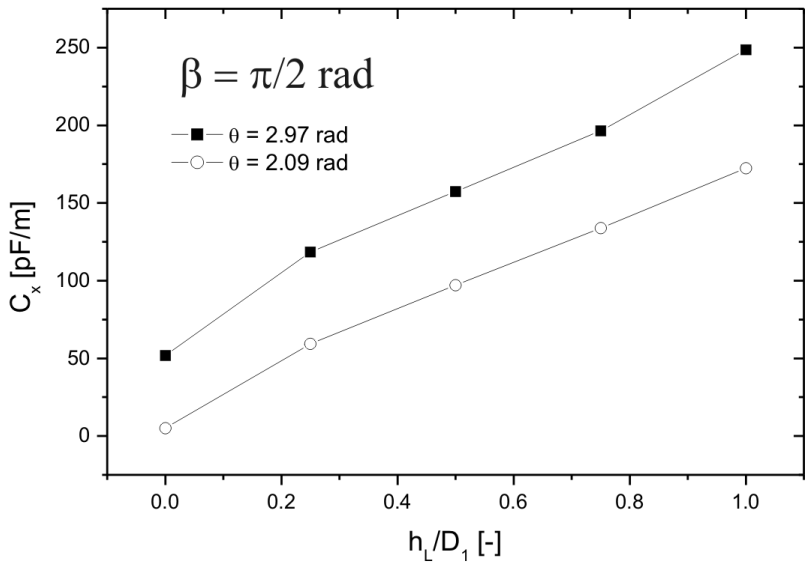

Figure 6. Capacitance C_x versus h_L/D_1 with $\beta = \pi/2$ radians

When $\theta = 2.09$ radians (empty cicle), some linearity occurred from $h_L/D_1 = 0.25$ to $h_L/D_1 = 1.0$, while it occurred only in the higher range of $h_L/D_1 = 0.0$ with the pipe full filled of air, therefore, C_x decreased from linear indicating that

the presence of bulk of water increased the potential gradients near the sensing electrode. Figure 7 shows electric potential distributions of both cases discussed, i. e., for $h_L/D_1 = 0$ and 1.0 and $\theta = 2.09$ radians, where the equipotential lines are more concentrate near the lower electrodes' edges in (b) when $h_L/D_1 = 1.0$. Additionally in Fig. 6, C_x varied about 200 pF/m from $h_L/D_1 = 0$ to 1.0 for $\theta = 2.97$ radians, while it varied about 150 pF/m for $\theta = 2.09$, showing a reduction on the probe's sensitivity as a consequence of the linearity obtained with $\theta = 2.09$.

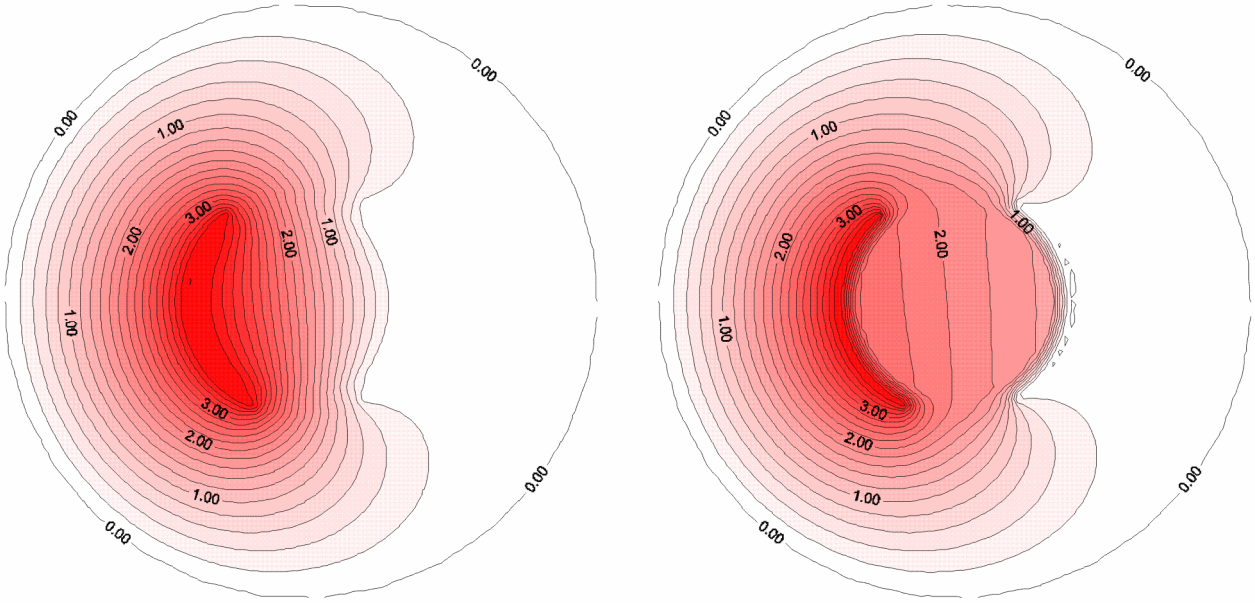

(a) β = π/2, θ = 2.09 rad and $h_L/D_1 = 0$ (b) β = π/2, θ = 2.09 rad and $h_L/D_1 = 1.0$

Figure 7. Distributions of Φ with the same θ and β and pipe full filled of air (a) and of water (b)

Figure 8 shows C_x as function h_L/D_1 for $\beta = 0$ radians, which is related to the Fig. 4 (c) and (d) also represented by the central point in the graph with $h_L/D_1 = 0.5$. In this case, there isn't linearity in the range of h_L/D_1 from 0 to 1.0 as expected by the series model. dos Reis and Goldstein Jr. presented similar experimental data from calibration of this kind of probe. The position of the sensor electrode on the top or on the bottom of the pipe surface had almost any effect of the probe's response. In both cases, C_x also varied about 200 pF/m from $h_L/D_1 = 0$ to 1.0 since θ was always 2.97.

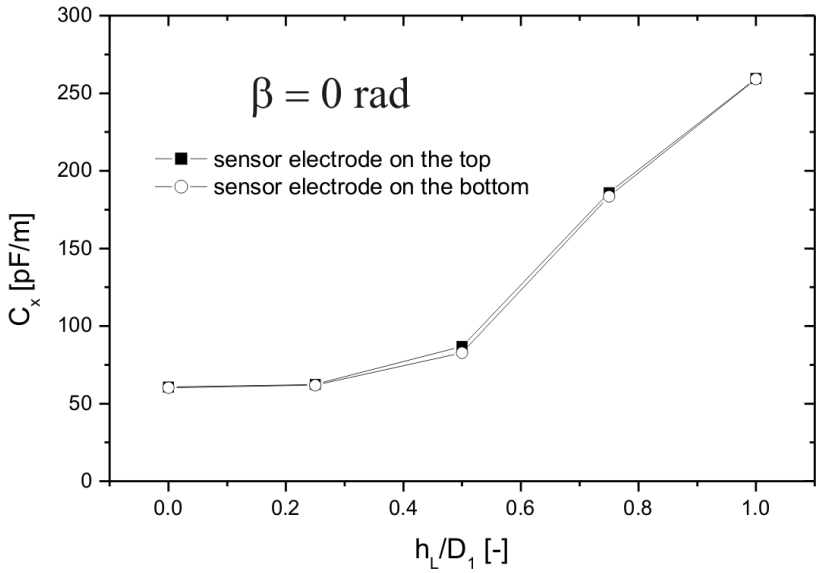

Figure 8. Capacitance C_x versus h_L/D_1 with $\beta = 0$ radians

Consider $\beta = \pi/2$ radians for liquid layer thickness measurement due to linearity is recommended, and still θ less than 2.97 radians (170°) to avoid deviations from linearity in the lower and upper range near $h_L/D_1 = 0$ and 1.0 due to

the pipe wall influence. However, there are other geometric effects present such as superficial tension in practical situations, which can curve the air-water interface also causing degradation of the probe response from the proposed numerical model (dos Reis, 2003).

6. CONSIDERATIONS ON CONDUCTIVE FLUIDS

The electromagnetic phenomena are described by the Maxwell's equations. Assumptions that the materials are isotropic and that the induced electromagnetic field has minor influence are sufficient to calculate distributions of the electric field through the Gauss' Law for the proposed capacitive probe (Hayt Jr. and Buck, 2001). However, if the presence of free electric charges into the probe's section was assumed, the equation to be solved is shown in Eq. (5) (Alme e Mylvaganam, 2006).

$$\vec{\nabla}.\left[\sigma(\vec{r})+ j\omega\varepsilon_o\ \varepsilon(\vec{r})\right]\vec{\nabla}\Phi(\vec{r})=0 \quad in \quad \Omega \tag{5}$$

Where Φ is the complex electric potential, σ is the electric conductivity of materials in S/m, $\omega = 2\ \pi f$ is the angular frequency in rad/s, f is the frequency of the excitation signal in Hz, and $j = \sqrt{-1}$.

There are two different assumptions that yield the Laplace's equation for the scalar electric potential Φ from Eq. (5), i. e., if σ = 0 S/m when the materials are perfectly dielectric as Eq. (1) or if $(\omega\varepsilon_o.\varepsilon) << \sigma$ when the conductive component is many times greater than the capacitive one, and Eq. (5) becomes Eq. (6), which is similar to Eq. (1) and, therefore, the same solution scheme discussed in item 3 can be used.

$$\vec{\nabla}.\left[\sigma(\vec{r})\vec{\nabla}\Phi(\vec{r})\right]=0 \quad in \quad \Omega \tag{6}$$

In practical situations of gas-liquid flows, the conductive component is many times greater than the capacitive one and Eq. (6) is valid. Consequently, if some amount of salt is dissolved in pure water, deviations on the capacitive probe response as presented in the item 3 can be observed. Verification of this statement was made by solving Eq. (6) for β = π/2 and θ = 2.97 radians for various h_L/D_1, similarly to the Fig. 6 (filled square).

If f is fixed and equal to 1 MHz, which is typical for capacitive probes, and σ and ε evaluated in this frequency, and with the assumption that it can be solved as a static field problem, the domain Ω can be divided in two parts: (A) from the shield screen to the inner pipe perimeter, including the annular space between the shield screen and the outer pipe perimeter, and the pipe wall region where the capacitive component is many times higher than the conductive one, and (B) into the pipe perimeter with two distinct regions, one filled of air where the capacitive component is many times higher and another filled of water with dissolved salts where the conductive component domains, and Eq. (1) or (6) can be solved, however, by using σ and ε as the electric property of each FEM element according to the dominant component: capacitive or conductive.

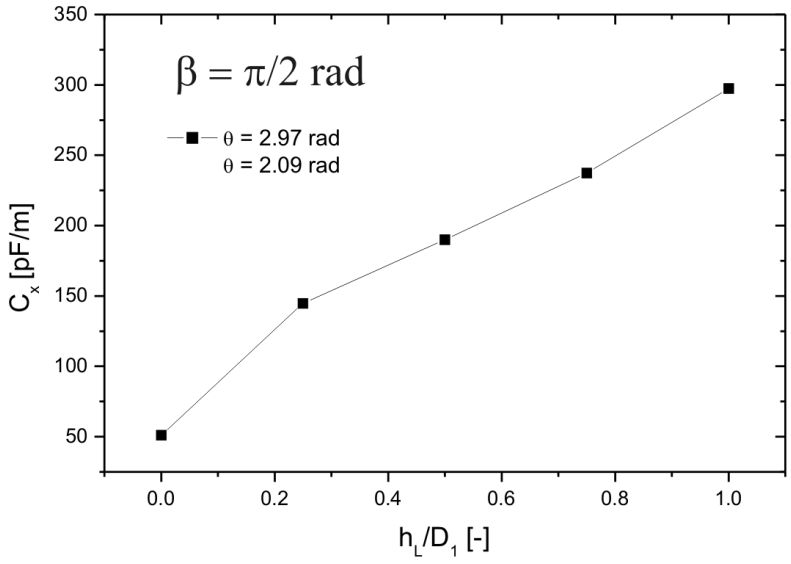

Figure 9. Capacitance C_x versus h_L/D_1 with β = π/2 radians for conductive water

For common water, $\sigma \cong 2\pi f\, \varepsilon'' \varepsilon_o \cong 225.9$ μS/cm according to the Debye's model (Raju, 2003), where ε'' is the dielectric dissipation factor and $\varepsilon'' = 406.1$ as determined experimentally by Galdiano (2010). Consequently, ε'' was about 5.1 times greater than the relative dielectric permittivity of water, and therefore, where the conductive component is dominant.

Figure 9 shows C_x, calculated for different h_L/D_1 with the electric property of the water equal to σ (or ε'') and the same values of dielectric permittivity presented in item 3 for air and Plexiglas, as function of h_L/D_1. The effect of the salt dissolved in the water was to increase C_x in all $h_L/D_1 > 0$, since all the electric potential gradient were into the pipe wall region as shown in Fig. 10, which means that any increase in the amount of salt shouldn't cause alteration on values of C_x. From Fig. 5 (filled square), Fig. 8 shows an increment of about 50 pF/m among all points with $h_L/D_1 > 0$ showing any variation of the probe's sensitivity. However, as C_x for $h_L/D_1 = 0$ was the same, a higher distortion from the linearity is lower region of the liquid layer thickness, while in the upper range there was any effective change in the probe's response, being still present the effect of the pipe wall as discussed before.

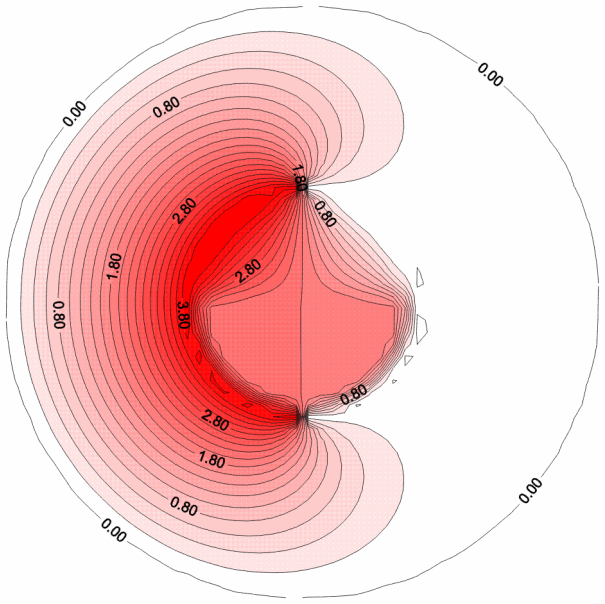

Figure 10. Distributions of Φ with $\theta = 2.97$, and $\beta = \pi/2$, $h_L/D_1 = 0.5$ and conductive water

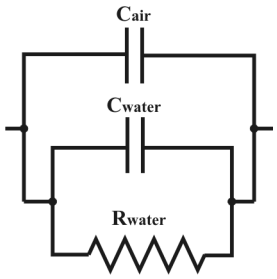

Figure 11. Flow section: $\beta = \pi/2$ and conductive water

Another result was an increment of C_x from about 250 to 300 pF/m (20% higher) while the electric property of the water increased from 80 to 406.1 (about 400% higher). In that sense, the flow section as in Fig. 5 is equivalent to the circuit shown in Fig. 11. The electric impedance represented by the pipe's wall is many times higher than other components, including the low electrical resistance represented by the bulk of conductive water. Consequently, C_x can't increase proportionally with the water electric property. It occurs only if electrodes are mounted internally to the pipe.

7. CONCLUSIONS AND REMARKS

This work presents a theoretical analysis based on Finite Element Method about a capacitance probe for measuring the water layer thickness in horizontal air-water two-phase piping flows, which extend the information about the probe proposed by dos Reis and Goldstein Jr. (2005). Differences due to temperature and compositions of materials must be considered in practical situations.

Four different configurations were tested: two different values of the electrodes' angle and two different positions in relation to the gravity, with simulations performed with different values of the water layer thickness from pipe full filled of air and to water. Therefore, 20 different simulations were performed assuming the materials into the measurement section as perfectly dielectric.

Consider a vertically electrodes' arrangement for liquid layer thickness measurement is recommended due to linearity observed in the probe response, and still an angle of the electrodes less than 2.97 radians (170^o) to avoid deviations from linearity in the lower and upper range due to the pipe wall influence. However, there are other geometric effects present such as superficial tension in practical situations, which can curve the air-water interface also causing degradation of the probe response from the proposed numerical model.

When conductivity is present into the water and electrodes are concave and mounted externally to the pipe, such as proposed in this work, it can increase the non-linearity of the probe mainly in the lower range of the liquid layer thickness, and also increase de range of capacitance to be measured. Additionally, the electric impedance represented by the pipe wall is many times higher than other components, including the low electrical resistance represented by the bulk of conductive water. Consequently, the capacitance can't increase proportionally with the electric property of the conductive water. It occurs only when the electrodes are mounted internally to the pipe

8. ACKNOWLEDGEMENTS

The support of FAPESP – Fundação de Amparo à Pesquisa do Estado de São Paulo, Brazil, is deeply appreciated.

9. REFERENCES

Alme, K. J., Mylvaganam, S, 2006, "Analyzing 3D and conductivity effects in electrical tomography systems using COMSOL multiphysics EM module". Proceedings of the 2006 Nordic COMSOL Conference, Copenhagen.

Demori, M., Ferrari, V., Strazza, D., Poesio, P., 2010, "A capacitive sensor system for the analysis of two-phase flows of oil and conductive water", Sensors and Actuators A: Physical, 163, pp. 172-179.

dos Reis, E., Goldstein Jr., L., 2005, "A non-intrusive probe for bubble profile and velocity measurement in horizontal slug flows", Flow Measurement and Instrumentation, 16, 4, pp. 229-239.

dos Reis, E., Goldstein Jr., L., 2010, "Characterization of slug flows in horizontal piping by signal analysis from a capacitive probe", Flow Measurement and Instrumentation, 21, 3, pp. 347-355.

dos Reis, E, 2003, "Study of pressure drop and phases distribution of the horizontal air–water slug flow in pipelines with "T" branch arms". Ph.D. Thesis, College of Mechanical Engineering, UNICAMP (in Portuguese).

Galdiano, E. S., 2010, "Contribution to the study of a non-invasive meter of water layer thickness in a annular oil-water core flow". Master Thesis, College of Mechanical Engineering, State University of Campinas, 2010 (in Portuguese).

Geraest, J. J. M., Borst, J. C, 1988, "A capacitance sensor for two-phase void fraction measurement and flow pattern identification". International Journal of Multiphase Flow, v. 14, n. 3, p. 305-320.

Haidari M., Azimi, P., 2011, "Conductivity Effect on the Capacitance Measurement of a Parallel-Plate Capacitive Sensor System", Research Journal of Applied Sciences, Engineering and Technology 3, 1, pp.53-60.

Hayt Jr, W. H., Buck, J. A, 2001, "Engineering Electromagnetics". Mc-Graw Hill, 6 ed., Boston, USA.

Jaworek, A., Krupa, A., Trela, M., 2004, "Capacitance sensor for void fraction measurement in water/steam flows", Flow Measurement and Instrumentation, 15, 5-6, pp. 317-324.

Kendoush, A. A., Sarkis, Z. A., 1995, "Improving the accuracy of capacitance method for void fraction measurements". Experimental Thermal and Fluid Science, 11, 4, pp. 321-326.

Keska, J. K., Fernando, R. D., 1992, "An experimental study of liquid film thickness measurement in a two-phase flow". AICHE Symposium Series, Heat Transfer, San Diego.

Niceno, B., 2008, "EasyMesh - A Two-dimensional Quality Mesh Generator". Available in: <http://www-dinma.univ.trieste.it/nirftc/research/easymesh/easymesh.html>, Accessed in February 5th of 2011.

Raju, G. G., 2003, "Dieletrics in Eletric Fields". Marcel Dekker, 1º ed., New York, USA.

Taitel, Y., Dukler, A. E., 1976, "A model for predicting flow regime transitions in horizontal and near horizontal gas-liquid flow". AIChE Journal, v. 22, n. 1, pp. 47-55.

Tollefsen, J. Hammer, E. A., 1998, "Capacitance sensor design for reducing errors in phase concentrations measurements". Flow Measurement and Instrumentation, 9, 1, pp. 25-32.

Xie, C. G., Stott, A. L., Plaskowski, A., Beck, M. S., 1990, "Design of capacitance electrodes for concentration measurement of two-phase flow". Measurement Science and Technology, 1, 65, pp. 65-78.

Yang, W. Q., 1996, "Hardware design of electrical capacitance tomography systems". Measurement Science and Technology, 7, 3, pp. 225-232.

10. RESPONSIBILITY NOTICE

The author is the only responsible for the printed material included in this paper.